Study on Mechanical Characteristics and Durability of Prestressed Anchorage Structure of Rock and Soil under Fatigue-Corrosion Coupling Action

Ming Li

School of Consturction Engineering, Zhengzhou Shengda University, Zhengzhou 450000, China
E-mail: Limingwang1027@hotmail.com

Received 12 April 2024; Accepted 27 May 2024

Abstract

This paper presents a comprehensive approach encompassing indoor experiments, theoretical analysis, and numerical simulations to investigate the durability of prestressed anchorage structures subjected to fatigue loads and corrosion. The study addresses the critical issue of gradual aging and damage caused by cumulative loads and corrosion, which ultimately leads to a decrement in structural durability. Through a rigorous analysis of the effects of fatigue load and corrosion on the performance of steel bars, numerical simulations were conducted to elucidate the failure mechanisms and variation patterns within the internal anchoring section. After subjecting steel bars to fatigue and corrosion tests for a defined duration, they were systematically categorized and exposed to varying fatigue tensile cycles in diverse acidic and alkaline environments. Employing the PFC2D program, a numerical model of the prestressed anchorage structure under the coupled effects of fatigue load, corrosion, and fatigue load was developed. This model allowed for a comparative analysis of the evolution of shear stress, axial stress, and displacement fields at the bolt-grout interface under two distinct conditions. The

European Journal of Computational Mechanics, Vol. 33_2, 145–172.
doi: 10.13052/ejcm2642-2085.3323

findings reveal the microscopic mechanisms underlying bond degradation at the bolt-grout interface under the synergistic impact of fatigue load and corrosion. The proposed methodology and experimental results demonstrate that geotechnical anchoring technology can effectively reinforce up to 70% of geotechnical structures, significantly reducing soil loss by approximately 80%. This research provides valuable insights into the durability of prestressed anchorage structures, paving the way for future improvements and optimizations.

Keywords: Prestressed anchorage structure, corrosion, fatigue load, durability, PFC2D.

1 Introduction

In recent years, geotechnical anchorage technology and its engineering application have developed rapidly. Applying anchoring technology to geotechnical engineering can improve the stability of rock and soil mass, reduce dead weight, reduce volume and control deformation. Geotechnical anchorage technology has obvious advantages and effects in strengthening geotechnical structures and solving complex geotechnical engineering problems [1, 2]. Rock and soil anchorage technology can be generally divided into prestressed anchorage and non-prestressed anchorage, in which prestressed anchorage technology embeds a part of the structure into stable rock and soil mass, so that the structure and stable deep rock and soil mass are bonded and embedded into a whole, and the other part of the structure is located on one side of unstable rock and soil mass. When unstable rock and soil mass produces displacement trend, the stress will be transmitted to stable rock and soil mass through anchorage structure, thus achieving the effect of strengthening unstable rock and soil mass with stable rock and soil mass, thus keeping the whole rock and soil mass stable [3].

Since 1960s, anchor rod has been widely used in various geotechnical engineering in China. After 1970s, anchor cable began to develop. From the initial introduction and application to now, the number of anchor structures has reached hundreds of millions. With the increase of its use quantity, its failure problem becomes more and more prominent [4, 5]. Generally, the working environment of anchor rod is very bad, and the surrounding environment is very easy to corrode steel bars [6]. Corrosion will reduce the mechanical properties of steel bars, make the surface of steel bars broken and

loose, and weaken the bond between anchor rod and grout. If we don't pay attention to the influence of corrosion on the mechanical properties of anchor rod and anchoring system, anchor rod will become a "time bomb", which will threaten the safety of engineering structures. At present, the research on the long-term durability of prestressed anchorage structures is not deep enough at home and abroad, and the reports on the long-term durability of anchorage structures are even more difficult to see. This is because the anchorage system, as a complex structure, is a concealed project buried underground, and it is difficult to monitor its construction quality and subsequent working conditions [7]. There are great differences in rock and soil in different projects, and the uncertainty of geological movement, external load and accidental load increases the difficulty of durability research.

The annual corrosion loss of every country in the world can account for $2\% \sim 4\%$ of the gross domestic product (GDP) on average. Among them, the corrosion loss in architectural engineering accounts for a large proportion (it is reported that it can account for more than 40%). According to the estimation of China's gross national product of 74 trillion yuan in 2016, the corrosion loss of buildings and infrastructure is about 1 trillion yuan [8, 9]. Although there is no more accurate statistical data about the damage caused by durability damage of anchorage structure, the economic loss and repair cost caused by it should not be underestimated.

For decades, international researchers have delved into the intricacies of durability, positioning it as a cornerstone in the field of geotechnical anchoring. However, domestic inquiries into this realm have lagged behind, with initial studies sparse and infrequent. In recent years, a surge in domestic research has been witnessed, yet the standards for designing and evaluating the long-term performance of anchor structures still fall short of perfection. Notably, C. A. Apostolopoulos et al. [10] embarked on accelerated corrosion tests on steel bars, uncovering a striking alignment between their corrosion outcomes and the real-world performance of corroded bars in engineering applications. Their investigations delved into the impact of corrosion on the ductility and mechanical properties of steel bars, highlighting that when exposed to a saline environment, these bars' mechanical capabilities plummet below the prescribed limits for reinforced concrete applications. This research landscape underscores the urgency for further exploration in this critical domain, particularly in the context of domestic research, where gaps in knowledge and standards remain. Bouteldja [11] evaluated the shear stiffness of anchor cables through numerical simulation, simulated

the interface between anchor cables and rock mass, and developed a new empirical model that takes into account the influence of factors such as anchor cable geometry, grouting quality, and confining pressure. A new design method was proposed for the load distribution of anchor cables, which showed good consistency with on-site results. Xia Ning [12] found that there is a significant difference in the damage of mortar protective layer between uniform and uneven corrosion. By constructing a model of corroded anchoring structure, the stress characteristics of the anchoring structure under the effects of confining pressure, anchoring force, and rust expansion force were analyzed, and the effects of corrosion and corrosion location on the bond and bearing capacity of anchor rods were studied. And ANSYS software was used for finite element analysis. In response to the shortcomings of existing methods, a durability evaluation method for corroded anchor solids based on fuzzy equivalence relationship was established. Wu Jin et al. [13] proposed a durability assessment method for concrete structures in the presence of Cl^- in the surrounding environment. A random distribution model of Cl^- concentration in concrete was established by taking the thickness of the protective layer and the Cl^- concentration on the concrete surface as random variables. The mean Cl^- concentration used to calculate the initiation time of steel corrosion was derived. And this method was used to evaluate the durability of the reinforced concrete guardrail on the west embankment of a certain harbor, verifying the consistency between the evaluation method and the on-site results. Li Shibin et al. [14] first accelerated the corrosion of steel bars, followed by axial fatigue stretching, and combined it with theoretical research. They found that under the combined effect of fatigue and corrosion, the life of steel bars will decrease, and the relationship between stress and fatigue life is logarithmic; As corrosion progresses, the attenuation of the fatigue curve can be divided into three stages: rapid increase, slow increase, and sudden increase. Wang Xianli et al. [15] comprehensively studied the rust expansion and crack development laws of reinforced concrete under the influence of various influencing factors through accelerated corrosion tests. The effects of various factors on the cracking time of rust expansion were found to be different, and the degree of influence was obtained. The specific influencing mechanisms of each factor were given, and measures to improve the durability performance of reinforced concrete structures were proposed. Zhu Jie et al. [16] established a finite element model using the extended finite element method and finite element software ABAQUS to simulate and analyze the rust expansion and cracking of concrete under non-uniform corrosion of steel bars. It was found that the model used can accurately

simulate concrete cracking and crack propagation; The grade of concrete and the thickness of the protective layer have an impact on the occurrence of rust expansion cracks. Increasing the grade of concrete and the thickness of the protective layer can improve the durability of the structure. Xu Gang et al. [17] used DIANA software to establish a simulation analysis model and conducted a comprehensive analysis of the cracking process of concrete protective layers caused by corrosion. A series of results were obtained, dividing the cracking process into four stages. The generation of cracks is related to the tensile strength of concrete, while the penetration of cracks is related to the thickness of the protective layer. In actual engineering, uneven rust expansion leads to slow corrosion of steel bars, and the spacing between steel bars and the thickness of concrete can affect the mode of concrete fragmentation.

To sum up, prestressed anchorage structure has many advantages compared with other engineering structures, and is widely used in various projects. However, under the coupling action of fatigue load and corrosion, its durability problem is very prominent, and a large number of failure cases have appeared, which have brought potential safety hazards and caused huge economic losses, which must be paid great attention to.

2 Performance Analysis of Steel Bar Under Coupling Action of Fatigue Load and Corrosion

2.1 Fatigue Failure in Corrosive Environment

After many times of alternating loads, the members of prestressed anchorage structure will be destroyed even if the alternating stress does not reach the yield limit of the members, which is called fatigue failure of the members. In the rolling process of general materials, there are always defects in the materials due to various reasons, and there will be some microcracks. Under the action of alternating load, these micro-cracks will gradually expand and accumulate, and then appear cracks on the macro level, which will eventually lead to failure when the macro-cracks develop to a certain extent. Fatigue failure is a complex process. Generally speaking, it can be divided into three stages: crack initiation, crack propagation and material fracture. The fatigue-corrosion coupling coefficient is formula (1):

$$\alpha = \frac{dN}{d\Delta K} exp\left(-\frac{Q}{RT}\right) \tag{1}$$

α is the fatigue corrosion coupling coefficient, which reflects the influence of corrosive environment on the fatigue crack propagation rate. dN is the increment of crack propagation length. $d\Delta K$ is the increment of stress intensity factor amplitude, Q is the corrosion activation energy, reflecting the relationship between the rate of corrosion reaction and temperature, R is the gas constant, and T is the absolute temperature.

In a corrosive environment, materials exhibit a propensity to fracture even under stress levels significantly below their fatigue threshold in normal atmospheric conditions, owing primarily to the accelerated crack propagation. The intricate nature of corrosion fatigue necessitates a comprehensive consideration of not only metallographic and mechanical factors but also electrochemical elements, rendering its fatigue behavior significantly more complex compared to atmospheric conditions. Notably, the emergence and progression of corrosion pits, the intercalation and dissolution of corrosion products during crack propagation, and the intricate interplay and distribution patterns of high-density cracks, constitute distinctive phenomena unique to corrosion fatigue that deserve special scrutiny.

2.2 Corrosion of Steel Bar

The service life of prestressed anchorage structure is the embodiment of the durability of anchorage structure, and corrosion directly threatens the durability of anchorage structure. The bolt body made of steel is mainly threatened by metal corrosion. In the natural environment, most metals cannot keep their elemental state, and they are easy to oxidize and corrode. Therefore, metal corrosion is a universal and spontaneous process, which is the reason why anchor rods often suffer from corrosion damage in practical engineering. Corrosion erodes the anchor rod, resulting in rust pits, rust spots, etc. on the surface of the rod body, and the volume of expanded rust will increase by 2 $\sim$ 4 times. Corrosion makes the anchor rod produce stress concentration at the weakening section of the material, thus accelerating the destruction of the anchoring structure and doing great harm to the anchoring structure. Coupled with the cyclic load, the corrosion of anchor rod will be aggravated.

Figure 1 shows the design principle of bolt body. According to the corrosion mechanism, the corrosion of anchor rod body can be divided into four types:

(1) Chemical corrosion, that is, the chemical reaction between the rod body and the surrounding medium, is not the main form of corrosion of anchor rod body;

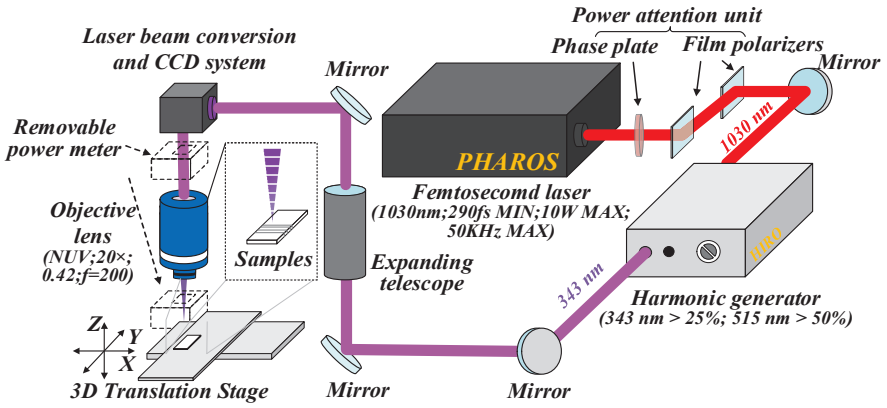

Figure 1 Design principle of bolt body.

(2) Electrochemical corrosion, in which current is generated in the reaction process, is similar to the state of battery, which depends on conductive solution to form corrosion battery. Electrochemical corrosion is the most common corrosion form of anchor rod;
(3) Physical corrosion, environmental factors and mechanical factors under the combined action of the accelerated destruction, physical corrosion can be divided into several types, and prestressed anchor generally for stress corrosion;
(4) Biological corrosion.

The pH value of mortar or concrete is generally greater than 12.5, which is strongly alkaline. However, when the pH value around the bolt is greater than 11, a dense (spinel solid solution) film with a thickness of about several nanometers will be formed on its surface, $Fe_3O_4 - Fe_2O_3$. Investigations have revealed that the protective film, which comprises silicon-oxygen bonds, possesses the capability to suppress the electrochemical reaction of steel bars. Even in the presence of water and oxygen, this film effectively safeguards the anchor rod from rusting. However, upon the disruption of this protective film, the bolt undergoes rapid corrosion. Notably, the reaction participants persist post-reaction, analogous to a catalyst, perpetually fueling the corrosion process of the anchor. The fundamental prerequisites for bolt corrosion are as follows: Firstly, a potential difference exists between the anode and cathode of the bolt; secondly, groundwater is rich in electrolytes, resulting in a low resistance of the electrolyte solution; and lastly, the protective film is compromised.

3 Study on Meso-change and Failure Law of Anchorage Section in Prestressed Anchorage Structure

3.1 Overview of PFC2D

The PFC2D particle flow program, rooted in the discrete element method, offers a powerful tool to simulate the intricate interplay, relationships, and interactions between spherical particles. In this framework, particles are granted the ability to move and rotate, enabling contact dynamics to unfold, which can be tailored to specific simulation needs through the selection of diverse contact types. Particles can be organized into groups and clusters, facilitating the assignment of unified values to these collective entities. Alternatively, particles can be assigned a common value based on their coordinate range or unique ID range. The program's measurement capabilities enable the precise tracking of stress, displacement, rotation, and other pertinent variables, both during and after simulations, either through the utilization of measuring circles or directly on individual particles. The PFC2D simulation relies on two fundamental assumptions: Firstly, the particle element is modeled as a rigid disk. Secondly, contacts are treated as flexible point contacts, with varying degrees of connection strength at each interface. The stress intensity factor of prestressed anchor cables, as depicted in formula (2), is a critical parameter in these simulations. Notably, PFC2D is adept at simulating large deformations, where particles are interconnected through bonds, enabling the simulation of complex physical phenomena with unprecedented accuracy.

$$\Delta K = Y\sigma_a\sqrt{\pi a} \tag{2}$$

In Equation (2), ΔK is the amplitude of the stress intensity factor of the prestressed anchor cable, reflecting the degree of stress concentration of the anchor cable under cyclic loading. Y is a geometric factor that is related to the shape and size of the anchor cable. σ_a is the stress amplitude of the anchor cable. A is half of the crack length.

3.2 Numerical Simulation Based on PFC2D Software

In the process of PFC2D software numerical simulation, firstly, the simulation object is defined, and the model is established according to the simulation intention and the simulation object. About each parameter, the key parameters are considered emphatically, while the irrelevant parameters are ignored appropriately. The model characteristic analysis sets reasonable stiffness, strength, size, specific gravity, contact and other characteristics for different

particles, walls and joints. Establishing and Running Test Model Before the establishment of test model, some test models should be tried out to find suitable parameters, which can be applied to the test model in the later period. Practical engineering modeling Practical engineering is complex. In simulation, it is necessary to simplify the practical problems to a certain extent and choose a reasonable parameter research range. Before running, the running time step is determined according to the actual engineering state and balance time. Generally, the model needs a lot of running time, which can be run on multiple computers and multiple windows at the same time, and record the working conditions of each window to avoid forgetting after running. After the preparation of running work is completed, when it is determined that the model file program is written correctly, the "call" command calls the data file for calculation [18]. Finally, the calculated results are compared with the measured results through the changes of stress, displacement and porosity.

Anchor technology is to fix one end of a tension rod in the rock or soil layer of a slope or foundation, and the fixed end of this tension rod is called the anchor end (or anchor section); The other end is connected to the engineering building and can withstand the thrust exerted on the building due to soil pressure, water pressure, or internal forces, utilizing the anchoring force of the stratum to maintain the stability of the building. Figure 2 is the structure diagram of steel corrosion fatigue crack extraction. This figure shows the main steps of extracting cracks from corrosion fatigue test samples, including: (1) cutting the test samples into several small pieces; (2) The position and shape of the crack are determined by metallographic

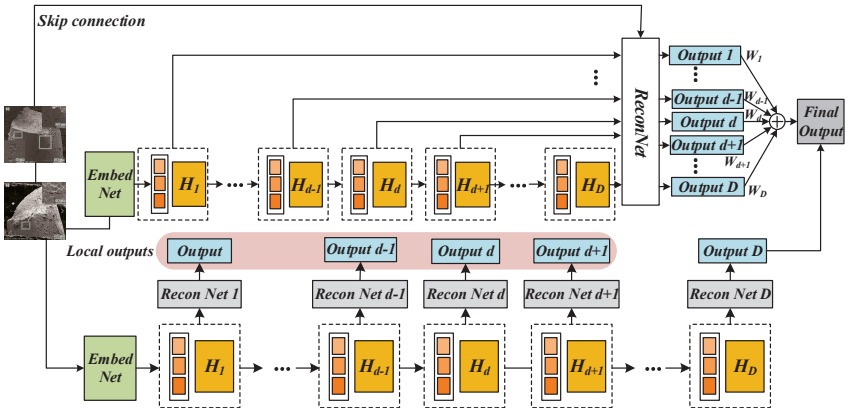

Figure 2 Structure diagram of corrosion fatigue crack extraction of steel.

observation in the crack area of the small sample; (3) Using electron beam welding technology to connect the crack area of small sample with a crack-free X65 steel plate to form a composite sample; (4) Drilling holes in the crack-free area of the composite sample to facilitate the subsequent tensile test; (5) Carry out tensile test on composite samples on universal testing machine to break the crack area; (6) Cracks were extracted from the fracture surface and observed and analyzed by scanning electron microscope.

3.3 Optimization Model of Prestressed Anchorage Structure in Rock and Soil

In our study, we focus primarily on elucidating the mesoscopic laws at the interface between the bolt and grout body. Given that the size and diameter of the grout body have minimal impact on the investigated phenomena, and the wide variance in bolt diameter to length ratios in practical engineering poses challenges for modeling, we have opted for a scaled-up approach in our test model. Specifically, the model bolt diameter is set at 0.5 meters, while the surrounding grout measures 8×8 meters, with an anchoring length of 7 meters. The horizontal dimension of the model aligns with the x-axis, while the axial direction of the anchor rod corresponds to the y-axis.

The modeling process commences with defining the boundary limits of our inquiry. Within these boundaries, grouting particles are generated along the walls, with some subsequently removed to accommodate the bolt particles, which are inserted at their intended locations and assigned distinct parameters [19, 20]. Notably, the prestressed steel bar experiences a synergistic effect of fatigue loading and corrosion, leading to surface rusting and expansion, which in turn increases the bolt diameter and diminishes the bond strength between the steel and grout. To simulate cyclic loading, alternating tensile forces are applied to the particles situated at the anchor rod's apex. Moreover, we manipulate particle parameters and introduce joints to emulate the evolution of steel bar rust expansion and bond strength degradation. This comprehensive approach enables us to gain a deeper understanding of the complex interplay between fatigue, corrosion, and material degradation at the bolt-grout interface.

Anchor technology is a sophisticated engineering method that involves embedding one end of a tension rod firmly within the rock or soil strata of a slope or foundation. This immobile terminus is referred to as the anchor end, serving as the pivotal point of stabilization. The opposing end is seamlessly integrated with the engineering structure, capable of enduring thrusts

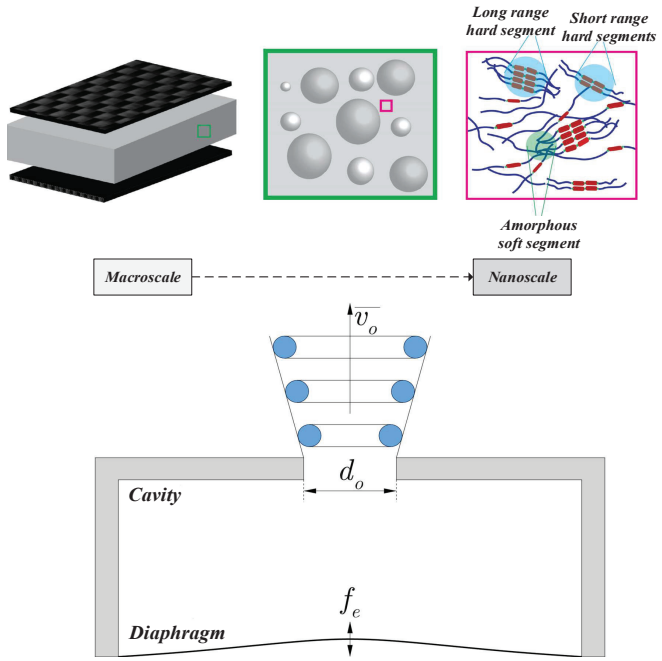

Figure 3 Deflection calculation flow of reinforced concrete beam under corrosion-fatigue coupling action.

imposed by soil pressure, water pressure, or internal forces, leveraging the inherent anchoring force of the strata to safeguard the structural integrity.

Illustrated in Figure 3 is a comprehensive deflection analysis framework for reinforced concrete beams subjected to the synergistic effects of corrosion and fatigue. The intricate interplay between the anchor rod and grouting body involves shear forces comprising adhesive force, mechanical bite force, and friction force. Notably, adhesive force emerges at the interface between the bolt and grouting body, constituting a significant portion of the tensile load under loading conditions. However, as the load intensifies, leading to slippage at the interface, the adhesive force dissipates.

The uneven or threaded surface of the anchor rod creates mechanical interlocks with the grouting body. In instances where extrusion contact occurs between the bolt and grouting body, and a relative displacement tendency emerges, friction comes into play, its magnitude dictated by the pressure and friction coefficient. The predictive models for fracture toughness and fatigue life of prestressed anchor cables, as depicted in Equations (3) and (4), provide

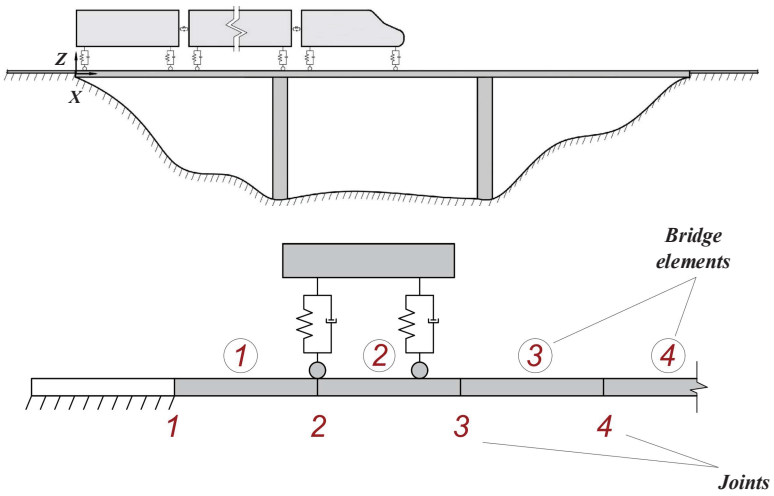

Figure 4 Conceptual model of geotechnical engineering.

valuable insights into the durability and longevity of this crucial engineering component.

$$K_c = \sigma_c \sqrt{\pi c} \tag{3}$$

$$N_f = \frac{1}{\alpha} \ln \left(\frac{K_c}{\Delta K} \right) \tag{4}$$

In Equation (3), K_c is the fracture toughness of the prestressed anchor cable, reflecting the anti fracture ability of the anchor cable. σ_c is the fracture stress of the anchor cable. c is half of the fracture length of the anchor cable. In Equation (4), N_f is the fatigue life of the prestressed anchor cable, reflecting the durability of the anchor cable under cyclic loading. K_c is the corrosion reaction rate constant, which is related to the properties and concentration of the corrosive medium.

The failure process of anchorage structure can be divided into three stages: elastic deformation, plastic deformation and debonding rolling: (1) elastic deformation [21, 22]. At the initial stage of tensile load application, and the tensile load is small; (2) Plastic deformation. With the increase of tensile load, the aggregate around the interface produces plastic deformation; (3) Debonding rolling. The tensile load continues to increase, and the aggregate changes from plastic deformation to breaking, and the aggregate has a rolling trend, and the interface mechanical properties change rapidly.

Figure 4 shows conceptual model of geotechnical engineering. PFC2D particle flow program can effectively simulate the shear stress composition at the interface between bolt and grout. A joint plane can be created between bolt particles and grout particles, and the contact and friction coefficient between particles can be added to the joint plane to simulate interfacial adhesion and friction [23, 24]. Particles with different concavity and convex are generated on the surface of bolt particles, which simulates the ribs and threads of bolt to form mechanical bite force. In the simulation of fatigue load in PFC2D, fatigue load is the load with varying size and direction in engineering, which can be divided into periodic load and aperiodic load. The calculation formulas of corrosion rate and corrosion depth of prestressed anchor cable are shown in Equations (5) and (6).

$$v_c = k_c C^n \tag{5}$$

$$d_c = v_c t \tag{6}$$

In Equation (5), v_c represents the corrosion rate of the prestressed anchor cable, reflecting the loss rate of the anchor cable in a corrosive environment. k_c is the corrosion reaction rate constant, which is related to the properties and concentration of the corrosive medium. C is the concentration of the corrosive medium. n is the order of corrosion reaction, reflecting the dynamic characteristics of corrosion reaction. In Equation (6), d_c represents the corrosion depth of the prestressed anchor cable, reflecting the degree of loss of the anchor cable in a corrosive environment. t is the corrosion time.

Fatigue load can be realized by controlling the magnitude of tensile load to change in constant amplitude near a specific stress value at any time step. The load spectrum is in the form of sine wave loading with 10% on the basis of tensile load, which changes every 10-time steps [25, 26]. In the method of determining cyclic loading times, the final state of the model operation should be that the system tends to be stable, which shows that the displacement changes smoothly, the time step-stress curve of each region tends to be horizontal, and the unbalanced force approaches zero. The method used in this model is to monitor the shear stress, that is, when the time step-shear stress curves at each position are close to the level, the model is considered to be in a stable state.

In the simulation of corrosion in PFC2D, it is found that after the corrosion of bolt, rust expansion will appear, which will have an impact on the bond between bolt and grout interface. According to the existing research results, the following settings are made in PFC2D: the volume change of rust

expansion is simulated by allowing the particles on the surface of anchor rod to expand, and the adhesion between joints can deteriorate with the progress of rust expansion by setting joints, because the adhesion between PFC2D particles can disappear with the change of displacement. Among them, the residual cross-sectional area of prestressed anchor cable and the residual tension formula of prestressed anchor cable are shown in Equations (7) and (8).

$$A_r = A_0 - \pi d_c D \tag{7}$$

$$T_r = T_0 \frac{A_r}{A_0} \tag{8}$$

In Equation (7), A_r is the remaining cross-sectional area of the prestressed anchor cable, reflecting the remaining bearing capacity of the anchor cable under corrosion and fatigue. A_0 is the initial cross-sectional area of the prestressed anchor cable. D is the diameter of the prestressed anchor cable. In Equation (8), T_r represents the remaining tensile force of the prestressed anchor cable, reflecting the remaining prestressing force of the anchor cable under corrosion and fatigue. T_0 is the initial tension of the prestressed anchor cable.

4 Experimental Results and Analysis

4.1 Shear Stress Analysis

The model can be divided into two working conditions: corrosive medium and non-corrosive medium. The shear stress changes of bolt-grouting interface and grouting body are monitored under various tensile loads until the shear stress of each measured circle is stable, and the shear stress curves are obtained by obtaining data, in which the tensile loads are divided into 9kN, 20kN, 40kN and 60kN. The shear stresses monitored in all measuring circles are not necessarily true values, because the measuring circles monitor the average shear stresses of all particles in the circles, while the particles in adjacent measuring circles may have different bonding states, rotation amounts and contact forces, which will affect the shear stress values, but they can still reflect the variation law of shear stresses [27].

The distribution of shear stress along the inner anchorage section is not homogenous, rather it is concentrated in the superior segment, manifesting a peak value at a distinct location. As tensile force escalates, the scope of this shear stress extends deeper into the inner anchorage section. In contrast

to other literature reporting inward movement phenomena, this simulation does not reveal such trends. This disparity arises from the fact that prior tests measured interfacial shear stress between the bolt and grouting body, whereas the present study captures shear stress proximal to this interface.

The shear stress's dynamics are intricately linked to both the transmission of anchoring force and the interplay of surrounding grouting particles, particularly those situated below. At low tensile loads, shear stress manifests in the superior segment of the inner anchorage section, with interfacial bond force assuming a pivotal anchoring role. However, as tensile loads incrementally surpass the interfacial bond strength of this superior segment, bond disruption occurs, and friction and mechanical bite forces take precedence. This combined resistance, alongside residual bond force, stabilizes the anchorage structure [28, 29]. However, as tension continues to surge to a critical threshold, the length of the inner anchorage section relying solely on friction and mechanical bite forces elongates, leading to a progressive inward expansion of shear stress, ultimately culminating in the collapse of the anchorage structure.

Although there is shear stress inward expansion phenomenon in both non-corrosion and corrosion conditions, the shear stress inward expansion under corrosion conditions is obviously faster than that under non-corrosion conditions, and the structure will lose stability earlier under external force, and the shear stress in each measuring circle under corrosion conditions is more different and fluctuates violently. This is because when there is corrosive medium at the interface, the particles of bolt and grout will become active, the bond at the upper part of the interface will be broken, and the tension load will be transferred downward, so more particles are needed to participate in the bond to resist the tension load.

Figure 5 shows the shear stress data at the anchor rod. The shear stress near the anchor rod is the largest and decreases rapidly outward. Shear stress is mainly distributed in the upper part of bolt, but there is basically no shear stress caused by tensile load in the lower part of bolt. Because of the self-weight of particles in the model, the monitoring of shear stress is affected, so the shear stress on the periphery and lower part of grouting body may be smaller.

Under the action of corrosion, the shear stress of grout decays faster transversely. Under the condition of corrosion, the grouting body at the measuring circle 4, that is, 0.5 m away from the anchor rod, can no longer effectively transfer the shear stress. Under the condition of non-corrosion, the grouting body within 1.2 m from the bolt can still transfer the shear

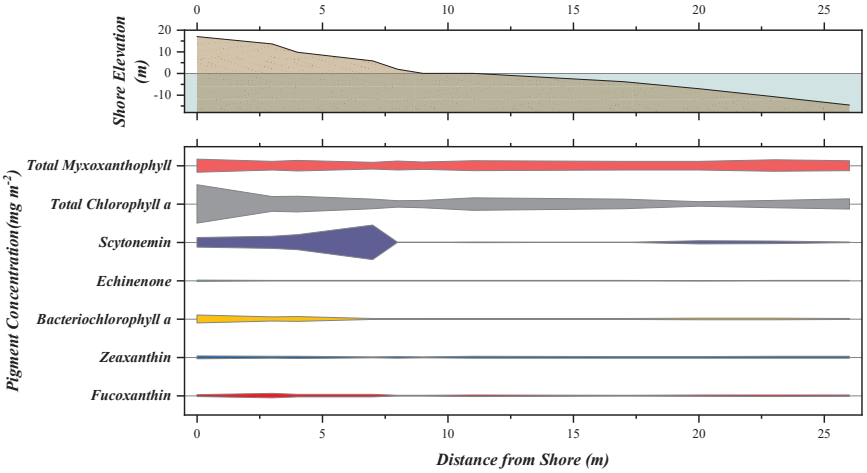

Figure 5 Shear stress data at bolt.

stress effectively in the measuring circle 10. The peak value of shear stress is 3800 Pa under corrosion condition, while the peak value of shear stress under non-corrosion condition is smaller than that under corrosion condition. At about 2800 Pa, the shear stress is scattered and the action range is large, and most areas of grouting body can participate in sharing shear stress. The calculation formulas of shear strength and ultimate bearing capacity of rock and soil are shown in Equations (9) and (10):

$$\tau = c + \sigma_n tan\varphi \tag{9}$$

$$q_u = N_c c + N_q q + N_\gamma \gamma B \tag{10}$$

In Equation (9), τ The shear strength of rock and soil reflects its shear resistance. c is the cohesion of the rock and soil, reflecting the cohesion of the rock and soil. σ_n is the normal stress of the rock and soil, reflecting the degree of compression of the rock and soil. φ is the internal friction angle of the rock and soil, reflecting the frictional properties of the rock and soil. In Equation (10), q_u represents the ultimate bearing capacity of the soil and rock, reflecting the bearing capacity of the soil and rock. N_c is the coefficient of influence on the cohesion of rock and soil, which is related to the internal friction angle of the rock and soil. N_q is the surface load influence coefficient of the rock and soil, which is related to the internal friction angle of the rock and soil. N_γ is the coefficient of influence on the self weight of rock and soil is related to the internal friction angle of the rock and soil. q is the surface

load of the rock and soil. γ is the bulk density of rock and soil. B is the width of the rock and soil.

The failure area of rock and soil and the calculation formulas of failure work of rock and soil are shown in Equations (11) and (12).

$$A_f = \pi DLsin\beta \tag{11}$$

$$W_f = \int_0^{A_f} \tau dA \tag{12}$$

In Equation (11), A_f is the failure area of the rock and soil, reflecting the failure range of the rock and soil. L is the length of the soil and rock. β is the failure angle of the rock and soil reflects the failure mode of the rock and soil. In Equation (12), W_f is the failure energy of the rock and soil, reflecting the failure energy of the rock and soil.

4.2 Displacement Analysis

It is also divided into two working conditions: non-corrosive medium and corrosive medium. The displacement changes of anchor rod and grout body under the working conditions of non-corrosive medium and corrosive medium are compared and analyzed when the tension load gradually increases [30]. Under the same load, the displacement of corroded anchorage system is faster than that of non-corroded anchorage system. Under the same load, the maximum displacement of corrosion anchoring system is larger than that of non-corrosion anchoring system. Except for the displacement when F = 9 kN, the maximum displacement of grouting body of corrosion anchoring system is also larger than that of non-corrosion anchoring system, which shows that corrosion reduces the bearing capacity of prestressed anchoring structure.

Figure 6 is a detailed analysis of the displacement dynamics within the rock-soil matrix under the coupled effects of fatigue and corrosion is presented. Notably, under minimal tensile loads, a distinct displacement inflection point emerges on the anchor rod. Above this point, the rod exhibits upward motion, whereas below it, a downward trajectory is observed. This phenomenon is attributed to the gravitational pull of the particles within the model, causing the lower section of the anchor rod to descend.

Our findings indicate that, at low tensile loads, only the upper segment of the anchor rod's anchorage section contributes significantly to the anchorage process, while the segment below the displacement inflection point plays

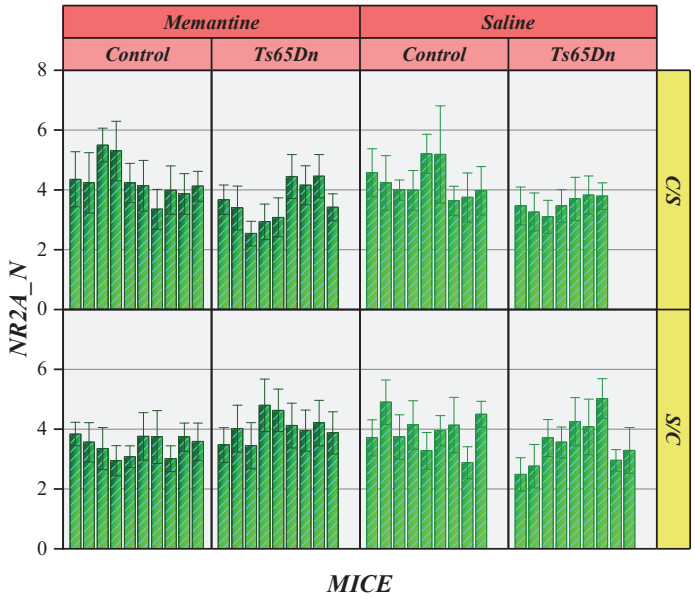

Figure 6 Displacement analysis of rock and soil under fatigue-corrosion coupling action.

a negligible role in the overall anchoring structure. When considering the failure mechanisms of anchoring systems, it becomes evident that cyclic loading alone leads to a widespread dissipation of anchoring forces within the grouting body. However, under the combined influence of cyclic loading and corrosion, failure manifests as a concentrated phenomenon at the bolt-grout interface, confined to a narrow region. This underscores the pivotal role of corrosion in affecting the durability of anchoring systems. Corrosion not only diminishes the load-bearing capacity of the system but also alters its failure pattern, making failures more concentrated and thus posing a greater threat to the overall durability. In contrast to non-corroded systems that tend to fail uniformly, corroded systems experience centric failures concentrated at the interface between the bolt and grouting body.

4.3 Axial Stress Analysis

A measuring circle is arranged in the bolt to monitor the axial stress distribution at each point along the bolt direction under the action of tension loads at all levels. Like shear stress, the axial stress on the bolt in the inner anchorage section is not uniformly distributed, and the axial stress in the upper part of

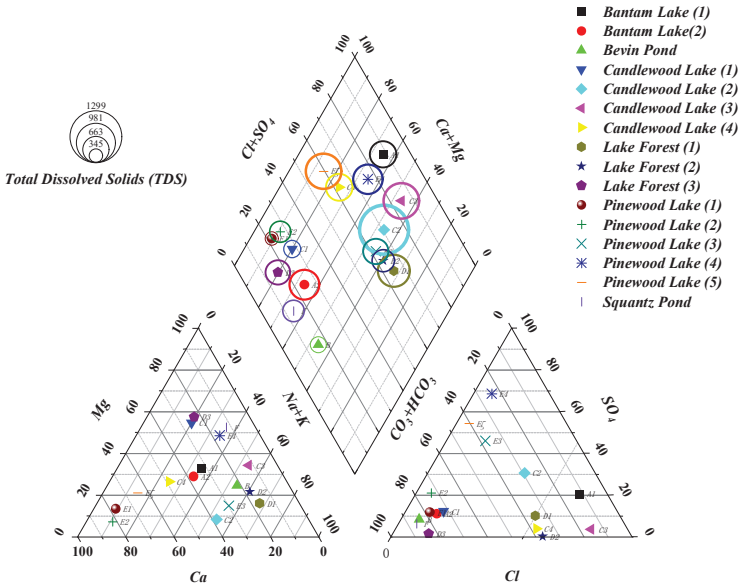

Figure 7 Corrosion analysis.

the inner anchorage section is the largest and gradually decreases along the bolt. This is because the grouting body around the upper part of the bolt and the surrounding rock mass share the stress of the bolt, so the axial stress of the bolt gradually decays to the depths. When the load increases, the maximum axial stress increases, and the range of axial stress gradually transfers to the lower end of the inner anchorage section, but the greater the load, the worse the effect of axial stress transfer, that is, the greater the load, the more concentrated the axial stress is at the front end of the inner anchorage section, and the smaller the relative axial stress transferred downward.

Figure 7 is a corrosion analysis. There is no obvious difference between the axial stress of bolt under non-corrosion and corrosion conditions. Within a certain range, with the increase of tension load, the axial stress will extend to the depth, and the friction and occlusion of the upper part of the anchorage section and the bonding effect of the deep part will be used to resist the tension load. However, when the tension load reaches a certain value, the grout particles in the upper part will be completely separated from the anchor rod, and the upper part of the inner anchorage section will not provide friction and occlusion, and the axial stress of the rod will shift downward until the structure is destroyed.

4.4 Fatigue Corrosion Test

This test is divided into two parts: fatigue loading test and corrosion test. Based on the corrosion test, this chapter continues to corrode the steel bar for 8 months. In the 6th, 8th, 10th and 12th months, the length, quality and diameter of the steel bar are measured and recorded for subsequent comparative analysis.

The surface of the rod body after corrosion for 1 month is shown as (a) and (b), and the surface of the rod body after corrosion for 12 months is shown as (c) and (d). The corrosion amount per unit length of each time node of steel bar is shown in Tables 1 and 2.

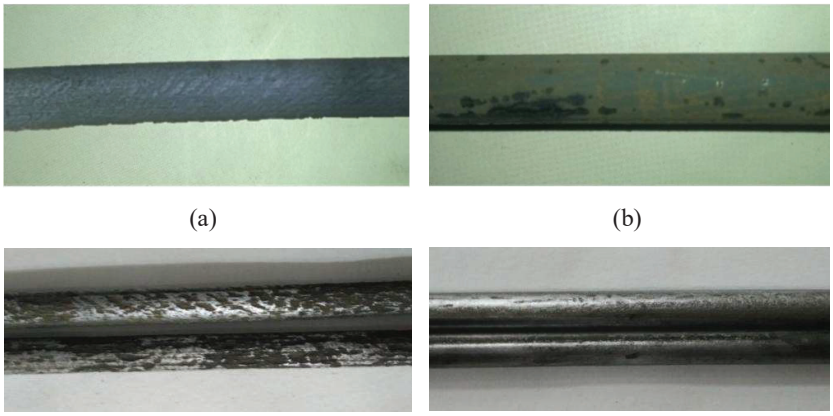

(a) (b)

(c) (d)

As can be seen from the figure, after one month of corrosion, the corrosion of steel bars is small, only shallow rust spots, which are basically uniform corrosion. After 12 months of corrosion, the surface of steel bars in acidic and alkaline environments is quite different. The rust spots showed different changes, and rust pits appeared on the surface of the rod, but the rust pits were deeper and more in obvious acidic environment. There will be stress concentration near the rust pit, which will lead to the yield of steel bars reaching tensile strength and fracture. Rust pit will affect the yield and ultimate bearing capacity of steel bars.

After the fatigue corrosion test is completed, four typical steel bar specimens are selected for tensile fracture. The specific selection method of specimens is shown in Table 3.

By observing the fracture surface of the selected specimens, the relationship between fatigue load and steel bar performance can be analyzed

Table 1 Corrosion data of acidic medium

Numbering	1 Month	2 Month	4 Month	6 Month	8 Month	10 Month	12 Month
A-0	0.05569	0.11351	0.20802	0.28229	0.32226	0.38972	0.44958
A-1	0.06027	0.12333	0.22468	0.3104	0.35269	0.41725	0.47074
A-2	0.06196	0.12924	0.23303	0.31675	0.33408	0.43316	0.5027
A-3	0.06080	0.12258	0.24504				
A-4	0.06393	0.13251	0.23926	0.34301	0.39559	0.42312	0.49607
A-5	0.06034	0.12421	0.22435	0.27645	0.30912	0.36436	0.42108
A-6	0.06282	0.12212	0.24312	0.30326	0.34308	0.4102	0.48657
A-7	0.06216	0.12534	0.24008	0.30597	0.36816	0.42045	0.48935
A-8	0.06550	0.13316	0.25138				
A-9	0.07163	0.14230	0.28925	0.37209	0.42616	0.4798	0.52319

Table 2 Corrosion data of alkaline medium

Numbering	1 Month	2 Month	4 Month	6 Month	8 Month	10 Month	12 Month
B-0	0.01462	0.03180	0.03621	0.06900	0.08689	0.10478	0.12267
B-1	0.01950	0.03143	0.03900	0.08331	0.10351	0.11866	0.14138
B-2	0.01676	0.03103	0.03895	0.09721	0.08724	0.13210	0.14955
B-3	0.01933	0.02866	0.04300	0.06259	0.07762	0.09264	0.12018
B-4	0.01627	0.03431	0.04024	0.06050	0.09923	0.12827	0.16215
B-5	0.01857	0.03036	0.04328	0.06485	0.07982	0.10227	0.11973
B-6	0.01913	0.02770	0.04123	0.06682	0.07671	0.09651	0.11383
B-7	0.01876	0.02997	0.04259	0.08317	0.09577	0.10585	0.11845
B-8	0.01607	0.02468	0.04327				
B-9	0.01873	0.02994	0.04435	0.07791	0.09550	0.13069	0.15833

Table 3 Scanning electron microscope test reinforcement selection

Specimen diameter	6.5 mm			
Corrosion time/month	12			
pH value	4	4	9	9
Previous loading times/times	0	80 thousand	5 thousand	80 thousand
Numbering	A-0	A-9	B-3	B-9

by pairwise comparison (A-0 and A-9, B-3 and B-9), and the relationship between acid-alkali environment and steel bar can also be analyzed by comparison (A-0 and B-3, A-9 and B-9). Stretch the selected A-0, A-9, b-3 and b-9 specimens until they break, and record the data during the tensile breaking process. The test model is SHT4605, as shown in (a), and the fracture surface after tensile breaking of steel bars is shown in (b).

(a) (b)

Upon the fracture of the steel bar, a rigorous cleaning procedure must be adhered to. Initially, the fracture site is thoroughly cleansed with distilled water to eliminate any impurities. Following this, the fracture is blown dry and subsequently placed in a dryer for optimal preservation. Prior to observation, a specimen of approximately 1 cm is delicately excised from the fracture surface, during which utmost care is exercised to safeguard the integrity of the fracture itself. Subsequent to an ultrasonic cleansing process in an alcohol solution, the fracture surface undergoes a comprehensive analysis, encompassing both macroscopic and microscopic perspectives. This analysis is conducted through scanning and photography using an advanced electron microscope (JSM-6610LA), which provides invaluable insights into the intricate relationship between fatigue load, corrosion, and the mechanical properties of the steel bars. The data pertaining to the tensile strength of the steel bars are presented in Table 4, offering a quantitative assessment of the material's performance.

Table 4 Tensile test data

Numbering	Yield Strength/ MPa	Yield Force/ KN	Maximum Force/ KN	Maximum Yield Strength Degrees/MPa	Original Gauge/ mm	After-break Gauge Distance/mm	Elongation/ mm
A-0	440	14.59	15.36	460	32.5	37	4.5
A-9	385	12.79	15.75	475	32.5	38	5.5
B-3	430	14.29	19.12	575	32.5	42	9.5
B-9	465	15.38	20.00	605	32.5	45	12.5

5 Summarize

Based on the theory of corrosion of steel bar and the method of fracture analysis, the fatigue corrosion test of steel bar is carried out firstly, and then some steel bars are pulled to fracture, and the macro and micro analysis of fracture surface is carried out, and the performance deterioration law of steel bar under the coupling action of fatigue load and corrosion is studied. The main conclusions are as follows:

(1) Corrosion per unit length of steel bar in acid-alkali environment has been increasing, and the daily increase is about 30%. Steel bar corrosion will occur in acid-alkali environment, and steel bar corrosion is a spontaneous process. The corrosion of steel bars in acid is faster than that in alkali, and the corrosion of steel bars is easier in acidic medium. Fatigue tensile damage the integrity of the surface of steel bars, resulting in cracks on the surface of steel bars, which will accelerate the corrosion of steel bars, but this conclusion still needs further research.

(2) The fracture characteristics of steel bars subjected to the coupling action of fatigue load and corrosion are quite different from those of normal steel bars. The deformation capacity of steel bar in acid environment is smaller than that in alkaline environment. The maximum load and yield strength of steel bar in acid environment are much smaller than those in alkaline environment. The corrosion of acid medium will reduce the deformation capacity and ultimate bearing capacity of steel bar.

(3) Through the macro and micro scanning of steel bar fracture surface, it is found that corrosive medium can invade steel bar in acid and alkali environment and produce corrosion products, but the corrosion is more serious in acid environment. Compared with alkaline environment, acid environment makes the deformation hardening index of steel bar increase, the plastic and mechanical properties decrease, and the internal structure is destroyed. The plasticity of steel bars with more fatigue tensile times is better. A certain number of fatigue loads can improve the plasticity of steel bars, which can increase the plasticity of steel bars to 200%.

(4) In model test, the meso-failure law in corrosive medium is quite different from that in non-corrosive medium. The reason is that when there is corrosive medium in the prestressed anchorage structure, the bolt expands, and the bonding force of the bolt-grout interface and the bolt surface decreases, which makes the particles at this interface become

active, resulting in the change of its mesoscopic failure law and the reduction of the bearing capacity of the anchorage system to about 80%.

References

[1] XiaoJian, X., GuangTao, X., Jian, Z., and Yu, C. (2024). Static and Dynamic Analysis of Coupled Vibration of Suspension Bridge Structure Under Earthquake Action. European Journal of Computational Mechanics, 32(06), 519–542.

[2] Naeij, M., Ghafarian, D., Ghasemi, H., and Javanmardi, Y. (2023). Experimental and numerical study on the dragged anchor–trenchless rock berm interaction. International Journal of Ocean and Coastal Engineering, 05(01n04).

[3] Mossalam, E., Ahmed, N. M., Souaya, E. M. R., and El-Sabbagh, B. (2020). The influence of binary pozzolanic replacements on the durability and corrosion performance of reinforced concrete. Pigment and Resin Technology, ahead-of-print(ahead-of-print).

[4] Kadhim, M. J., Al-Jadiri, R. S., and Ali, M. A. A. W. (2019). Study the effect of addition nano-tio2 by dispersion method on the some mechanical properties and durability of cement mortar. IOP Conference Series: Materials Science and Engineering, 518(3), 032027 (11pp).

[5] Wang, P., Xu, C., Li, Q., Guo, Y., and Wang, L. (2023). Evaluation on the mechanical, thermal insulation and durability properties of wood recycled ecological concrete. Materialia, 32.

[6] Peng, Y., and Zhou, S. (2024). Mechanical Behavior Analysis of High Strength Concrete Beams in Architectural Design: Simplified Calculation Method of Flexural and Shear Bearing Capacity. European Journal of Computational Mechanics, 32(06), 543–566.

[7] Zhang, N., Wang, H., Wang, S., Wang, S., Guo, Y., and Xun, X. (2023). Experimental study on the evolution law of pore structure and mechanical properties of mudstone under the effect of water rock chemistry. Journal of Porous Media.

[8] Gao, Y., Wang, Y., Lu, T., Li, L., Wu, J., and Zhang, Z. (2021). An experimental study on the mechanical properties of high-temperature granite under natural cooling and water cooling. Advances in Materials Science and Engineering.

[9] Feng, M. U., Zi-Min, C., Yu-Ling, L. I., Xue-Hua, X. U., Xiao-Gang, L. I., and Forestry, C. O. (2019). Study on the biomechanics and

fatigue characteristics of single root soil and soil of tree roots in taihang mountain. Journal of Northwest Forestry University.

[10] Apostolopoulos, C. A., and Papadakis, V. G. (2008). Consequences of steel corrosion on the ductility properties of reinforcement bar. Construction and Building Materials, 22(12), 2316–2324.

[11] Bouteldja, M. (2000). Design of cable bolts using numerical modelling.

[12] Xia Ning (2005). Preliminary Study on Mechanical Properties and Durability Evaluation of Rusted Anchor Solids (Doctor dissertation, Nanjing: Hohai University).

[13] Wu Jin, and Wu Shengxing (2005). Durability life assessment of reinforced concrete structures under chloride ion environment Journal of Civil Engineering, 38(2), 59–63.

[14] Li Shibin, Zhang Weiping, Gu Xianglin,&Zhu Cimian (2010). Accelerated fatigue test research on corroded steel bars Journal of Railways, 32(5), 5.

[15] Wang Xianli,&Zheng Jianjun (2009). Experimental study on rust expansion cracking and crack propagation in reinforced concrete structures Journal of Dalian University of Technology, 49(2), 246–253.

[16] Zhu Jie,&Fang Congqi (2013). Extended finite element numerical analysis of rust expansion and cracking in concrete structures Mechanics Quarterly (1), 9.

[17] Xu Gang, Xu Ke, Wang Qing, and Wang Yimin (2012). Simulation analysis of the entire process of rust expansion and cracking in reinforced concrete structures Journal of Building Materials, 15(3), 7.

[18] Zhang, H., Meng, X., and Yang, G. (2020). A study on mechanical properties and damage model of rock subjected to freeze-thaw cycles and confining pressure. Cold Regions Science and Technology, 103056.

[19] Damijan, Z., Peitang, W., and Nikola, V. (2024). The effect of gear-manufacturing quality on the mechanical and thermal responses of a polymer-gear pair. Journal of Computational Design and Engineering.

[20] Zhang, J., Li, M., Lin, G., and Di, K. (2021). Study on dynamic mechanical properties and failure mechanism of sandstones under real-time high temperature.

[21] Michailidis, N., Stergioudi, F., Ragousis, A., Lopez-, H., and Castaneda. (2019). A study on corrosion-fatigue behavior of aa7075-t651 subjected to different surface modification treatments. Fatigue and Fracture of Engineering Materials and Structures.

[22] Bermeo-Campos, R., Madrigal-Carrillo, K., Perez-Figueroa, S. E., Calvino, M., Trejo, A., and Salazar, F., et al. (2023). Surface morphology effects on the mechanical and electronic properties of halogenated porous 3c-sic: a dft study. Applied Surface Science: A Journal Devoted to the Properties of Interfaces in Relation to the Synthesis and Behaviour of Materials (Sep.15), 631.

[23] Huang, L., Du, Y., Qi, H. H., and Wang, Y. (2023). Mechanical properties and constitutive model of filling medium in hot casting socket at elevated temperatures. Construction and Building Materials (Dec.8), 408.

[24] Gibalenko, O., Gibalenko, V., and Bocharova, O. (2020). Anticorrosive protection of structures in robust design. MatSciRN: Localized Corrosion (Topic).

[25] Hailin, W., Linhai, L. U., Guofu, W., and Hong, S. (2019). Study on microstructure and fractal features of shallow ground in jinan. Yellow River.

[26] Yingzi, H., and Ruilin, L. (2019). Study on the effect of recycled aggregate on mechanical properties and durability of concrete. Cement Engineering.

[27] Zhifang, M., Shihao, Z., and Xiaoguang, G. (2024). Analysis on Shear Resistance of Joint and Structural Mechanical Response of Assembled Composite Beam Joints. European Journal of Computational Mechanics, 32(06), 589–608.

[28] Yayuan, H. U. (2018). Effect of double-variable coupling on the fluctuating characteristics of unsaturated rock and soil. Journal of Vibration and Shock.

[29] Boga, A. R., and Senol, A. F. (2023). The effect of waste marble and basalt aggregates on the fresh and hardened properties of high strength self-compacting concrete. Construction and Building Materials (Jan.11), 363.

[30] Shangguan, M., Xie, Y., Wang, F., Long, G., Tang, Z., and Chen, Y., et al. (2023). Effect of low-vacuum environment on the strength and permeability of cement-based materials. Construction and Building Materials (Oct.12), 400.

Biographies

Ming Li received the Bachelor's degree in Engineering from Tongji University in 2006, the Master's degree in Engineering form Nanjing University of Science & Technology in 2016. He is currently working as a lecturer at the School of construction engineering Zhengzhou Shengda University. His research areas and directions include mechanics, materials, and structures.

Project approval number:

242400410247

Name of Project:

Research on the Action Mechanism and Spatial Effect of Digital Economy Driving High-quality Urban Development in Henan Province under the New Development Pattern;
Zhengzhou Shengda University.